Signature of an ultrafast photoinduced Lifshitz transition in the nodal-line semimetal ZrSiTe

Robert J. Kirby,[1] Lukas Muechler,[2] Sebastian Klemenz,[1] Caroline Weinberg,[1] Austin Ferrenti,[1] Mohamed Oudah,[1,3] Daniele Fausti,[1,4,5] Gregory D. Scholes,[1] and Leslie M. Schoop[1,*]

[1]*Department of Chemistry, Princeton University, Princeton, New Jersey 08544, USA*
[2]*Center for Computational Quantum Physics, The Flatiron Institute, New York, New York 10010, USA*
[3]*Quantum Matter Institute, University of British Columbia, Vancouver, British Columbia, Canada V6T 1Z4*
[4]*Department of Physics, Università degli Studi di Trieste, Trieste I-34127, Italy*
[5]*Sincrotrone Trieste S.C.p.A., Basovizza, Trieste I-34012, Italy*

(Received 6 November 2020; accepted 27 April 2021; published 19 May 2021)

Here we report an ultrafast optical spectroscopic study of the nodal-line semimetal ZrSiTe. Our measurements reveal that, converse to other compounds of the family, the sudden injection of electronic excitations results in a strongly coherent response of an A_{1g} phonon mode that dynamically modifies the distance between Zr and Te atoms and Si layers. "Frozen phonon" density functional theory calculations, in which band structures are calculated as a function of nuclear position along the phonon mode coordinate, show that large displacements along this mode alter the material's electronic structure significantly, forcing bands to approach and even cross the Fermi energy. The incoherent part of the time-domain response reveals that a delayed electronic response at low fluence discontinuously evolves into an instantaneous one for excitation densities larger than 3.43×10^{17} cm^{-3}. This sudden change of the dissipative channels for electronic excitations is indicative of an ultrafast Lifshitz transition, which we tentatively associate with a change in topology of the Fermi surface driven by a symmetry-preserving A_{1g} phonon mode.

DOI: 10.1103/PhysRevB.103.205138

I. INTRODUCTION

Light can be a powerful driving force in physical and chemical transformations; photoexcitation above a certain threshold fluence can often induce the same phase transitions at ambient conditions that would normally require, for example, high temperature, such as the metal-to-insulator transition in VO_2 [1–4] or charge-density-wave melting in $LaTe_3$ [5]. Importantly, most photoinduced phase transitions (PIPTs) are associated with a structural symmetry breaking. Photoexcitation can also nonadiabatically access regions of a material's potential energy surface that equilibrium stimuli cannot, leading to the possibility of new transformations that would be inaccessible with other external stimuli [6–8]. Ultrafast laser experiments provide access to out-of-equilibrium PIPTs. Furthermore, ultrafast pump-probe spectroscopic techniques allow one to follow the progress of the PIPT, either directly (as with near-field optical techniques [9]) or indirectly (e.g., through the contribution of certain coherent phonon modes and their fluence dependence [3]). This can provide very powerful insight into the mechanism through which the phase transition occurs, and it can help to tailor any potential applications to a certain phase transition and vice versa.

Recently, indications of a Lifshitz transition—a peculiar electronic phase transition in which the topology of the Fermi surface changes without an accompanying change in crystal symmetry [11]—have been observed in high-pressure Raman and equilibrium reflectance experiments on the nodal-line semimetal (NLSM) ZrSiTe, supported by density functional theory (DFT) calculations [12,13]. In these experiments, pressure was applied along the c-axis of the material, forcing the atomic layers of the material closer together. The evidence supporting the electronic phase transitions were discontinuities in the screened plasma frequency (extracted from Kramers-Kronig analysis of the equilibrium reflectance spectra) and the nonlinear response of the frequency of an A_{1g} phonon mode. The DFT calculations indicated that at high pressure, bands cross the Fermi energy along Γ-X and Γ-M.

The ZrSiX (X = S,Se,Te) family of materials are the archetypal NLSMs, and they have presented themselves as a particularly active area of research in recent years, especially ZrSiTe. Crystallizing in the PbFCl structure type, in the $P4/nmm$ space group, these materials consist of layers of X and Zr on either side of a Si square net, i.e., X-Zr-Si-Zr-X. Their band structures are characterized by large-bandwidth nodal-line bands near the Fermi energy, which are relatively free from interference from trivial bands. All three ZrSiX compounds also display nonsymmorphic symmetry-protected Dirac crossings at the X-point, and although these crossings are hundreds of meV above and below the Fermi energy in ZrSiS and ZrSiSe, they occur at E_F in ZrSiTe [14]. ZrSiTe also has weaker interlayer bonding than the other ZrSiX members [15], behaving like a quasi-2D material [16]; it can be exfoliated down to few-layer sheets [17], and the monolayer is predicted to be a topological insulator [15]. Additionally, topological drumhead surface states were recently observed for the first time in ZrSiTe [18], distinguishing it

*lschoop@princeton.edu

from ZrSiS where only trivial surface states are experimentally observable [19]. Staying within the family, electronic correlations were recently shown to exist in ZrSiSe [20], and a temperature-induced Lifshitz transition has also been proposed [21] in the same compound.

Other topological semimetals (TSMs) have been shown to exhibit Lifshitz transitions, including $ZrTe_5$ [22], VAl_3 [23], NbAs [24], TaP [25], TaAs [25], WTe_2 [26], $NiTe_2$ [27], $PtTe_2$ [28], and T_d-$MoTe_2$ [29]. Most Lifshitz transitions have been observed to occur in equilibrium, induced by a wide range of stimuli including temperature, pressure and strain, and material composition. However, the correlated Weyl semimetal T_d-$MoTe_2$ stands out as being the only material found to undergo a nonequilibrium Lifshitz transition [30]. An ultrafast near-infrared (NIR) laser pulse was used to excite the material, and the subsequent change in the Fermi surface was observed with time- and angle-resolved photoemission spectroscopy (tr-ARPES). Ultrafast spectroscopy has been shown to be such a useful tool in inducing and tracking the evolution of other varieties of electronic and structural phase transitions; it is surprising that there is a dearth of examples of its applicability to Lifshitz transitions.

Here we present a combined experimental and computational study of the ultrafast optical response of ZrSiTe, showing that ZrSiTe is only the second topological semimetal and the first nodal-line semimetal to undergo a PIPT. This article has the following structure: first, transient reflectivity shows that a strong relationship exists between the electronic subsystem and the lattice through a particular phonon mode. Next, DFT "frozen phonon" calculations of the band structure as a function of nuclear position along the phonon mode coordinate show that intense excitation of this phonon mode can have drastic effects on the material's band structure, potentially resulting in a Lifshitz transition. Returning to the transient reflectivity experiments, the signature of an ultrafast PIPT is observed in the fluence dependence of the incoherent part of the transient response, that is, the response of bulk thermalized electrons upon which the oscillatory motion of the coherent phonon is overlaid. While these experiments cannot cast light on the precise nature of the PIPT and the topology of the resulting Fermi surface, the strong excitation and computations suggest that we might be witnessing an ultrafast nonequilibrium Lifshitz transition, as well as a new mechanism by which the transition is mediated by fully symmetric coherent phonons.

II. EXPERIMENTAL METHODS

Single crystals of ZrSiTe were grown by chemical vapor transport. Zirconium sponge (Sigma Aldrich, 99%) silicon pieces (Sigma Aldrich, 99.95%) and cleaned tellurium crystals were stoichiometrically mixed, and small amounts of iodine (Alfa Aesar, ultradry 99.999%) were added. The cleaned tellurium crystals were obtained by chemical vapor transport using tellurium pieces (Sigma Aldrich, 99.999%). The elements were sealed in a quartz ampoule *in vacuo*. The tube was placed in a tube furnace, heated to 1100 °C in 6 h, and held at that temperature for 7 days. After this time, the samples were removed at temperature and quenched in water. Single crystals of ZrSiSe and ZrSiS were grown using previously reported methods [10,31]. Representative crystals were ground to a powder and analyzed using a STOE STADI P x-ray diffractometer (Mo $K\alpha 1$ radiation, Ge monochromator). Chemical analysis was done using an XL30 FEG-SEM equipped with an Oxford EDX detector. The EDX analysis confirms the composition of the material (see Fig. S1 of the Supplemental Material) [32].

Transient reflectivity experiments were performed with a commercial pump-probe setup (Ultrafast System Helios). The 1.55 eV output from a 1 kHz regeneratively amplified Ti:sapphire laser (Coherent Libra) was split with a 50:50 beamsplitter to produce both the pump and probe pulses. Narrowband pump pulses centered at 1.24 and 0.95 eV were produced in an optical parametric amplifier (OPerA Solo). Broadband NIR probe pulses covering 0.8–1.35 eV were produced by focusing the 1.55 eV light in a sapphire crystal. A $\lambda/2$-waveplate, a polarizer, and an iris control the polarization, intensity, and shape of the beam used to produce the probe pulse. The pulses strike the sample at near-normal incidence, and the reflected probe light is collected by a fiber optic and sent to the detector. All samples were measured in the *ab* plane, and all measurements were performed at room temperature.

ZrSiTe is air-sensitive, and was kept in an argon-filled glovebox. Transient measurements were performed with the single crystals enclosed in an air-tight sample holder, which was also prepared in the Ar-filled glovebox. The transient measurements on the ZrSiSe—which is also air-sensitive—and ZrSiS single crystals were performed in the same fashion.

The raw transient data are background-corrected to remove pump scatter from the data. This is accomplished by averaging the response at each probe energy over the negative delay times (when the probe pulse reaches the sample before the pump pulse) and subtracting the average from the entire response at each probe energy. The data are also chirp-corrected to remove the effects of the chirp that the probe pulse collects as it is produced. This is done using the Helios software SURFACE XPLORER. Points are chosen along the coherent artefact, where the chirp is most noticeable, and fit with a polynomial function, which is subsequently subtracted ensuring that all probe energies along the polynomial—and thus the coherent artefact—have the same relative delay time.

To analyze the coherent oscillations and the underlying incoherent response—which together form the entirety of the transient response—separately, we fit the transient at each probe energy with a sixth-order polynomial over all positive delay times. The order of the polynomial is low enough that the fit only captures the nonoscillatory incoherent response and misses the highly oscillatory features of the coherent part. Therefore, we take the polynomial fit to be the incoherent part. Subtracting the fit from the overall response leaves the just coherent part; the frequencies present here can then be analyzed with a fast Fourier transform (FFT).

The Raman spectrum of ZrSiTe was collected with a Horiba Raman microscope. The sample was excited with unpolarized 532 nm light incident on the *ab* plane, and scattered light from the same plane was collected by the microscope objective.

"Frozen phonon" DFT calculations were performed using the VASP and PHONOPY packages [33,34] with the standard

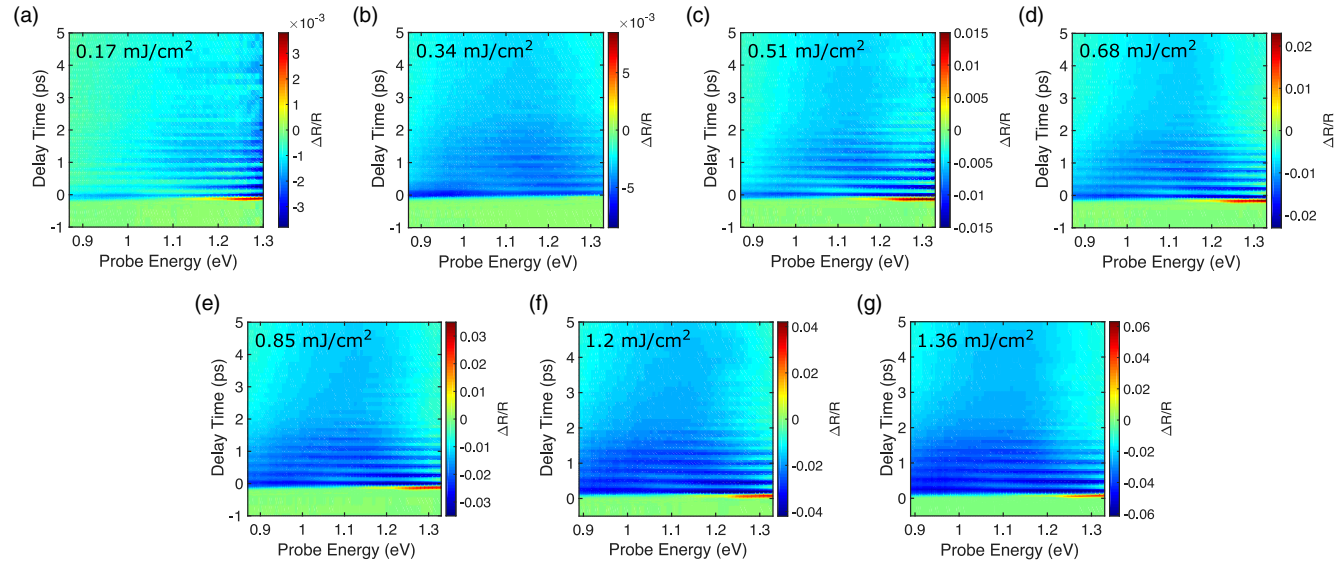

FIG. 1. The transient response of ZrSiTe pumped at 1.24 eV at fluences of (a) 0.17 mJ/cm^2, (b) 0.34 mJ/cm^2, (c) 0.51 mJ/cm^2, (d) 0.68 mJ/cm^2, (e) 0.85 mJ/cm^2, (f) 1.2 mJ/cm^2, and (g) 1.36 mJ/cm^2. An oscillatory response is clearly visible at all fluences, arising from the excitation of a coherent A_{1g} phonon mode as discussed in the text. The $\frac{\Delta R}{R}$ scale was chosen to emphasize that the entirety of the signal, save for the coherent artefact at 0 ps delay time, is negative, which is in contrast to the transient response when pumped at 1.24 eV in the same spectral range for ZrSiSe and ZrSiS, which exhibit both negative and positive features, the latter arising from lattice heating subsequent to hot carrier cooling [10].

pseudopotentials for Zr, Si, and Te. The experimental geometries were taken from Ref. [35]. For the self-consistent calculations, the reducible Brillouin zone (BZ) was sampled by a $9 \times 9 \times 7$ k-mesh, and spin-orbit coupling was included. The one-electron energies were calculated as a function of the A_{1g} normal mode coordinate, assuming the adiabatic Born-Oppenheimer approximation.

III. RESULTS AND DISCUSSION

The transient response of ZrSiTe pumped at 1.24 eV over almost an order of magnitude of fluences can be seen in Fig. 1. In this response, large oscillations due to the excitation of coherent phonons are superimposed on top of the bulk incoherent electronic response of the material. The FFT spectrum of the oscillations in Fig. 1(f) as a function of probe energy is presented in Fig. 2(a), showing that a single phonon mode is being excited; the FFT amplitude increases with increasing probe energy—possibly approaching a resonance—but it does not completely disappear at the lower end of the probe window. The coherent phonons dephase after 2 ps.

The phonon frequency extracted from the FFT spectrum, 125 cm^{-1}, corresponds to an A_{1g} phonon mode also observed in steady-state Raman experiments [Fig. 2(b)]; the mode is depicted in Fig. 2(c). This mode brings the Zr and Te atoms closer to [Fig. 2(c)], and farther away from (not shown), the Si square net relative to their equilibrium positions. No additional modes appear above or below a certain fluence, which suggests that ZrSiTe does not undergo a photoinduced change in symmetry within our fluence range. The frequency of the 125 cm^{-1} A_{1g} phonon mode is roughly 15 cm^{-1} higher than that observed in bulk samples in other studies [13,17]. This is possibly due to slightly different compositions or carrier concentrations resulting from crystals grown in different labs. However, the frequency is consistent between our transient reflectivity and steady-state Raman measurements. These experiments were also repeated using a lower energy pump pulse, 0.95 eV. These additional data are presented in Figs. S3 and S4 [32]. At both pump energies and at all fluences, the same sole 125 cm^{-1} Raman mode was observed, with similar relative amplitudes.

The coherent phonon response can be seen more clearly in the transient data at a single probe energy, 1.15 eV, in Fig. 2(d). The self-same A_{1g} coherent phonon mode has also been observed in the transient reflectivity spectra of ZrSiSe and ZrSiS when pumped with 0.95 eV photons [Figs. 2(e) and 2(f)]. In these materials, the mode has a frequency of 150 and 220 cm^{-1}, respectively. However, the amplitude of the oscillations in these materials is minuscule compared to those in ZrSiTe, and in experiments in which ZrSiSe and ZrSiS were pumped with 1.24 eV photons, no coherent oscillations were observed. Furthermore, these materials only exhibit coherent phonons when pumped at high fluence—1.2 mJ/cm^2 for ZrSiSe and 1.7 mJ/cm^2 for ZrSiS—which is not the case for ZrSiTe. Although Te's large polarizability, relative to those of Se or S, is undeniably a contributing factor in the enhanced Raman response compared to the other two materials, it is highly unlikely that this wholly accounts for the significant increase in amplitude. The large amplitude of the coherent phonons relative to the incoherent electronic response—tens of percent in the first period—suggests that this mode is being strongly excited.

A recent study predicts that the geometry of this phonon mode, in which the distance between the Zr and Te atoms and the Si square net is changing, should have a strong impact on the stability of the nodal-line structure [36]. To explore this, we performed "frozen phonon" DFT calculations. The results of the calculations are separated by the phase of the phonon

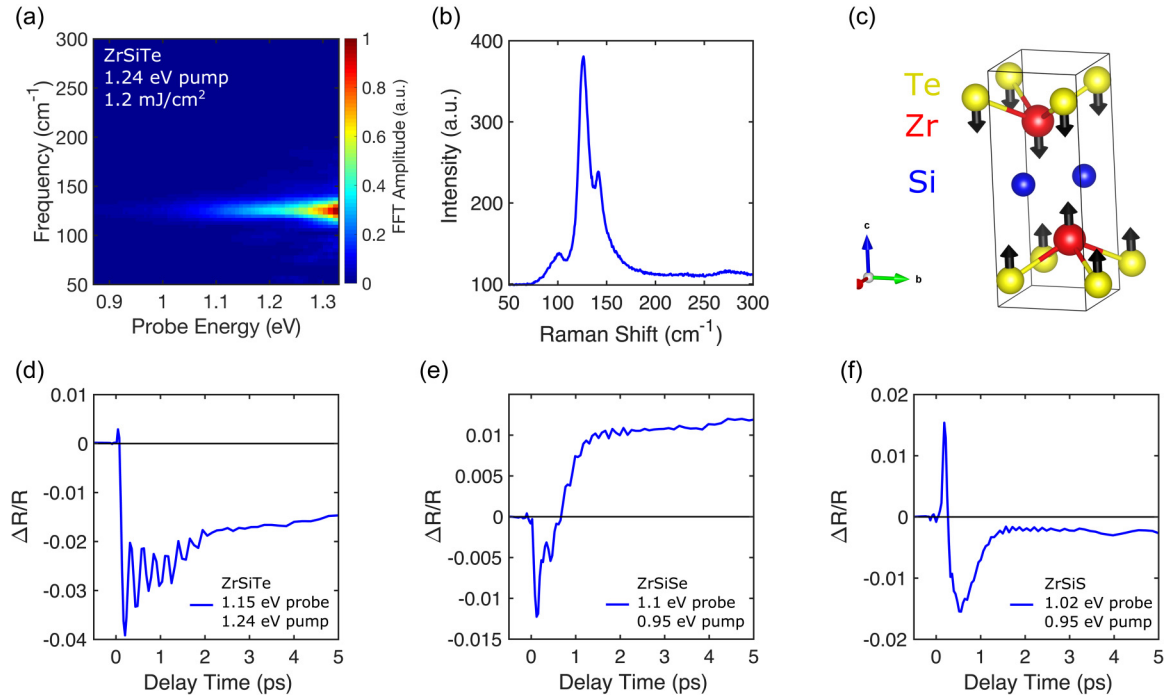

FIG. 2. (a) FFT spectrum of the oscillatory response for ZrSiTe pumped at 1.24 eV at a fluence of 1.2 mJ/cm^2 [Fig. 1(f)] as a function of probe energy, showing a single frequency at 125 cm^{-1}, corresponding to an A_{1g} phonon mode. This mode is also on prominent display in the Raman spectrum of ZrSiTe, (b). (c) The crystal structure of ZrSiTe (blue, Si; red, Zr; and yellow, Te) showing one phase of the A_{1g} phonon mode, in which the Zr and Te atoms approach the Si square net from either side; in the other phase of the phonon mode (not shown), the Zr and Te atoms move further away from the Si square net relative to their equilibrium positions. (d) The transient response of ZrSiTe pumped at 1.24 eV, 1.2 mJ/cm^2, at a probe energy of 1.15 eV. In the first few periods of the coherent phonon, the amplitude of the oscillatory part is quite large, tens-of-percent of the total magnitude. This is in contrast with the same singular coherent phonon mode observed in ZrSiSe [(e) pumped at 0.95 eV, 1.2 mJ/cm^2, probed at 1.1 eV] and ZrSiS [(d) pumped at 0.95 eV, 1.7 mJ/cm^2, probed at 1.02 eV]. The coherent phonon response in ZrSiTe is significantly stronger than in either ZrSiSe or ZrSiS.

motion. The effects of the Te and Zr atoms moving toward the Si square net (compared to their equilibrium positions) on the band structure are shown in Fig. 3(a), herein referred to as "negative distortions," and the effect of the atoms moving further away from the Si square net (again compared to equilibrium), or "positive distortions," in Fig. 3(b). The change in Si-Te distance in the crystal structure due to displacement along the phonon mode is used as a metric for the amount of distortion.

Focusing first on the effects that negative distortions have on the band structure [Fig. 3(a)], we can see that there are two noticeable changes in the vicinity of the Fermi energy. At high displacement, Te p-states increase in energy toward E_F between Γ and X, almost touching E_F at the highest

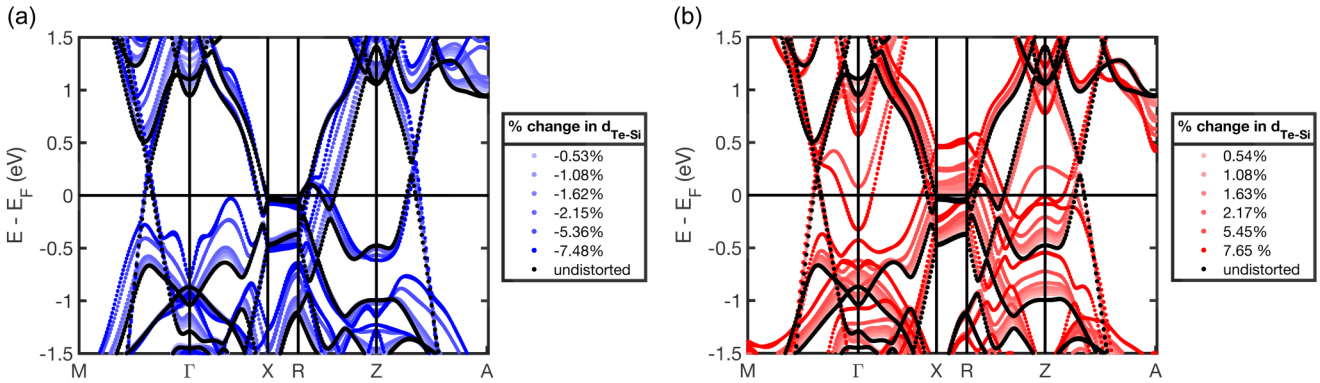

FIG. 3. Band structures for ZrSiTe for various displacements along the coherent A_{1g} phonon mode. Part (a) shows the effects of displacements which bring the Zr and Te atoms closer to the Si square net, relative to the equilibrium positions, and (b) shows the effect of the Zr and Te atoms moving further away from the Si square net, relative to their equilibrium positions. The displacement direction in (a) is that displayed in Fig. 2(c). At high displacements—measured by the change in the Si-Te distance—bands approach and cross E_F; ZrSiTe is predicted to undergo Lifshitz transitions along both phases of the coherently excited A_{1g} phonon mode.

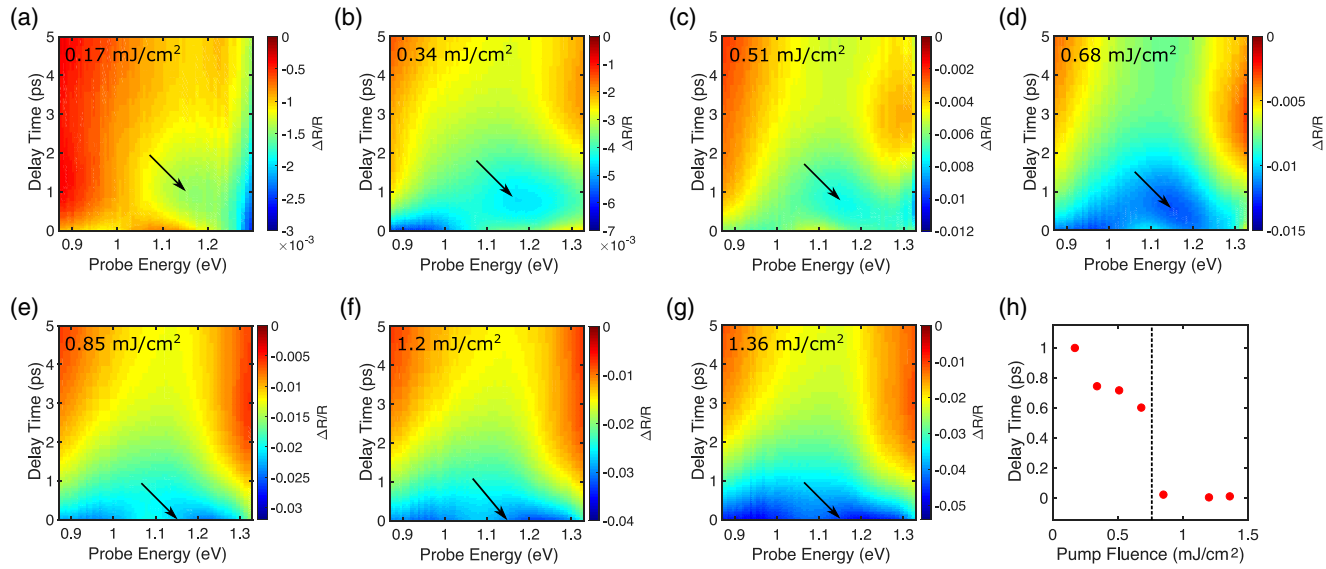

FIG. 4. The incoherent parts extracted from the transient data for ZrSiTe pumped at 1.24 eV with fluences of (a) 0.17 mJ/cm^2, (b) 0.34 mJ/cm^2, (c) 0.51 mJ/cm^2, (d) 0.68 mJ/cm^2, (e) 0.85 mJ/cm^2, (f) 1.2 mJ/cm^2, and (g) 1.36 mJ/cm^2. Arrows emphasize the minima in these incoherent parts at 1.15 eV probe energy. Part (h) illustrates how these incoherent minima fall into two different fluence regimes. Below 0.75 mJ/cm^2, the delay time at which the minimum is observed decreases linearly with increasing pump fluence; there is a discontinuity at the threshold fluence 0.75 mJ/cm^2, after which the minima are observed at 0 ps delay time, independent of increasing pump fluence. This is the signature of an ultrafast PIPT discussed in the text.

amplitude studied. Additionally, the nodal-line bands between R and Z, primarily composed of Si p- and Zr d-states, shift closer to R and to higher energy even at modest distortions. Both of these band shifts would alter the Fermi surface. Other changes to the band structure occur further away from E_F and are of little consequence to our experimental results.

Moving now to the effects of the positive distortions [Fig. 3(b)], two striking features stand out. The first can be seen at Γ, where a band approaches E_F from above, eventually crossing below it at the highest displacement studied. The second is at Z, where bands increase in energy through E_F. Other shifts in the energy and momentum position of the nodal-line bands can be seen between R and Z, similar to those observed at negative distortions.

These data indicate that ZrSiTe potentially undergoes Lifshitz transitions at the extrema of both phases of the phonon mode observed in the transient data. Due to the strong excitation of this mode, these distortions along the phonon mode are not believed to be unrealistic. The higher negative distortions were chosen to be the Si-X, X = (S, Se), distances in ZrSiX (3.532 Å for ZrSiS and 3.615 Å for ZrSiSe, compared with 3.891 05 Å for ZrSiTe). These ranges are based on a comparative assessment of different compounds in this family of materials and on known crystallographic constraints for these compounds.

To show that the large phonon displacement might drive a Lifshitz transition, we analyze the bulk incoherent electronic response that we mentioned earlier. Figures 4(a)–4(g) show these extracted incoherent responses for all fluences when pumped at 1.24 eV; the incoherent parts of the 0.95 eV experiments can be found in Fig. S5 [32]. The incoherent parts of the lower fluence experiments [Figs. 4(a)–4(d)] reveal a minimum in the data roughly 1 ps after the pump and probe pulses overlap, at a probe energy of 1.15 eV. However, no such delayed minimum appears in the high fluence incoherent parts [Figs. 4(e)–4(g)]; here the minimum occurs right at 0 ps. Plotting the delay time at which these minima occur [Fig. 4(h)], we can see that there are two distinct regimes: for fluences below 0.75 mJ/cm^2, the delay time minimum decreases linearly with increasing fluence, whereas above 0.75 mJ/cm^2 the minimum occurs during excitation by the pump pulse, independent of fluence. The same phenomenon is observed in the 0.95 eV pump experiments, however here the threshold fluence is lower, 0.42 mJ/cm^2 (Fig. S5) [32].

This behavior, in which there are distinct regimes of a quantity (here the incoherent minimum delay time) separated by a threshold fluence or excitation density, is indicative of a PIPT. The threshold fluences correspond to excitation densities of 3.43×10^{17} cm^{-3} (1.24 eV) and 2.71×10^{17} cm^{-3} (0.95 eV). The increase in threshold excitation density with increasing pump energy is almost perfectly mirrored by a decrease in absorbance: 0.0315 (1.24 eV) compared with 0.0417 (0.95 eV), meaning fewer photons need to be absorbed to provide the required energy to complete the phase transition immediately. One might wonder whether this threshold behavior could also conceivably arise from laser-induced damage (i.e., the sample is gradually damaged as the pump fluence is increased, and above a certain fluence no more damage can be inflicted, resulting in the observed threshold behavior). However, this is an unlikely interpretation of our observation. Measurements were not performed sequentially with increasing fluence but rather in random order, so the threshold behavior cannot stem from a gradual increase in the amount of irreversible damage with fluence. Furthermore, we observe no changes to the frequencies present in the coherent phonon FFT spectra with increasing fluence, which suggests that the

structural symmetry of the material remains intact and that any modifications to the material are largely electronic in nature.

IV. CONCLUSION

Transient reflectivity measurements on the NLSM ZrSiTe show that NIR pulses can strongly excite one particular 125 cm^{-1} A_{1g} phonon mode—coherently—on top of the bulk incoherent electronic response. DFT studies showed that large displacements along this phonon mode adjust the band structure so significantly that bands approach and cross E_F, abruptly changing the Fermi surface such that the material undergoes a Lifshitz transition. Furthermore, the fluence dependence of the incoherent part of the transient response has the hallmark of an ultrafast PIPT, with a threshold fluence of 0.75 mJ/cm^2 when pumping with 1.24 eV photons and 0.42 mJ/cm^2 when pumping with 0.95 eV photons. The large-amplitude coherent phonons give credence to the displacements required to undergo a Lifshitz transition by DFT; however, further studies are necessary to show whether the signature of an ultrafast PIPT observed in the transient data corresponds to this Lifshitz transition or arises from some other ultrafast electronic transition. Moreover, we elucidated this picture within the intuitive Born-Oppenheimer approximation, but in reality the nuclear and electronic degrees of freedom are likely coupled. The possibility of an ultrafast photoinduced Lifshitz transition could make ZrSiTe an ideal candidate material for high-frequency photoswitchable optoelectronic devices, but it also presents ZrSiTe as a potential system from which to gain a better understanding of this exciting class of ultrafast PIPT.

ACKNOWLEDGMENTS

This work was supported by NSF through the Princeton Center for Complex Materials, a Materials Research Science and Engineering Center DMR-2011750, by Princeton University through the Princeton Catalysis Initiative, and by the Gordon and Betty Moore Foundation through Grant No. GBMF9064 to L.M.S. G.D.S. is a CIFAR Fellow in the Bio-Inspired Energy Program. D.F. was supported by the European Commission through the European Research Council (ERC), Project INCEPT, Grant No. 677488. The authors also acknowledge the use of Princeton's Imaging and Analysis Center, which is partially supported by the Princeton Center for Complex Materials, a National Science Foundation (NSF)-MRSEC program (DMR-2011750). The Flatiron Institute is a division of the Simons Foundation.

[1] A. Cavalleri, T. Dekorsy, H. H. W. Chong, J. C. Kieffer, and R. W. Schoenlein, Evidence for a structurally-driven insulator-to-metal transition in VO_2: A view from the ultrafast timescale, Phys. Rev. B **70**, 161102(R) (2004).

[2] C. Kübler, H. Ehrke, R. Huber, R. Lopez, A. Halabica, R. F. Haglund, Jr., and A. Leitenstorfer, Coherent Structural Dynamics and Electronic Correlations During an Ultrafast Insulator-To-Metal Phase Transition in VO_2, Phys. Rev. Lett. **99**, 116401 (2007).

[3] S. Wall, D. Wegkamp, L. Foglia, K. Appavoo, J. Nag, R. Haglund, J. Stähler, and M. Wolf, Ultrafast changes in lattice symmetry probed by coherent phonons, Nat. Commun. **3**, 1 (2012).

[4] D. Wegkamp, M. Herzog, L. Xian, M. Gatti, P. Cudazzo, C. L. McGahan, R. E. Marvel, R. F. Haglund Jr., A. Rubio, M. Wolf, and J. Stähler, Instantaneous Band Gap Collapse in Photoexcited Monoclinic VO_2 Due to Photocarrier Doping, Phys. Rev. Lett. **113**, 216401 (2014).

[5] A. Zong, A. Kogar, Y.-Q. Bie, T. Rohwer, C. Lee, E. Baldini, E. Ergeçen, M. B. Yilmaz, B. Freelon, E. J. Sie, H. Zhou, J. Straquadine, P. Walmsley, P. E. Dolgirev, A. V. Rozhkov, I. R. Fisher, P. Jarillo-Herrero, B. V. Fine, and N. Gedik, Evidence for topological defects in a photoinduced phase transition, Nat. Phys. **15**, 27 (2019).

[6] H. Ichikawa, S. Nozawa, T. Sato, A. Tomita, K. Ichiyanagi, M. Chollet, L. Guerin, N. Dean, A. Cavalleri, S.-i. Adachi, T.-H. Arima, H. Sawa, Y. Ogimoto, M. Nakamura, R. Tamaki, K. Miyano, and S.-Y. Koshihara, Transient photoinduced 'hidden' phase in a manganite, Nat. Mater. **10**, 101 (2011).

[7] L. Stojchevska, I. Vaskivskyi, T. Mertelj, P. Kusar, D. Svetin, S. Brazovskii, and D. Mihailovic, Ultrafast switching to a stable hidden quantum state in an electronic crystal, Science **344**, 177 (2014).

[8] T.-R. T. Han, F. Zhou, C. D. Malliakas, P. M. Duxbury, S. D. Mahanti, M. G. Kanatzidis, and C.-Y. Ruan, Exploration of metastability and hidden phases in correlated electron crystals visualized by femtosecond optical doping and electron crystallography, Sci. Adv. **1**, e1400173 (2015).

[9] S. A. Donges, O. Khatib, B. T. O'Callahan, J. M. Atkin, J. H. Park, D. Cobden, and M. B. Raschke, Ultrafast nanoimaging of the photoinduced phase transition dynamics in VO_2, Nano. Lett. **16**, 3029 (2016).

[10] R. J. Kirby, A. Ferrenti, C. Weinberg, S. Klemenz, M. Oudah, S. Lei, C. P. Weber, D. Fausti, G. D. Scholes, and L. M. Schoop, Transient Drude response dominates near-infrared pump-probe reflectivity in nodal-line semimetals ZrSiS and ZrSiSe, J. Phys. Chem. Lett. **11**, 6105 (2020).

[11] I. M. Lifshitz, Anomalies of electron characteristics of a metal in the high pressure region, JETP **11**, 1130 (1960).

[12] J. Ebad-Allah, M. Krottenmüller, J. Hu, Y. L. Zhu, Z. Q. Mao, and C. A. Kuntscher, Infrared spectroscopy study of the nodal-line semimetal candidate ZrSiTe under pressure: Hints for pressure-induced phase transitions, Phys. Rev. B **99**, 245133 (2019).

[13] M. Krottenmüller, M. Vöst, N. Unglert, J. Ebad-Allah, G. Eickerling, D. Volkmer, J. Hu, Y. L. Zhu, Z. Q. Mao, W. Scherer, and C. A. Kuntscher, Indications for Lifshitz transitions in the nodal-line semimetal ZrSiTe induced by interlayer interaction, Phys. Rev. B **101**, 081108(R) (2020).

[14] A. Topp, J. M. Lippmann, A. Varykhalov, V. Duppel, B. V. Lotsch, C. R. Ast, and L. M. Schoop, Non-symmorphic band degeneracy at the Fermi level in ZrSiTe, New J. Phys. **18**, 125014 (2016).

[15] Q. Xu, Z. Song, S. Nie, H. Weng, Z. Fang, and X. Dai, Two-dimensional oxide topological insulator with iron-pnictide

superconductor LiFeAs structure, Phys. Rev. B **92**, 205310 (2015).

[16] J. Hu, Z. Tang, J. Liu, X. Liu, Y. Zhu, D. Graf, K. Myhro, S. Tran, C. N. Lau, J. Wei, and Z. Mao, Evidence of Topological Nodal-Line Fermions in ZrSiSe and ZrSiTe, Phys. Rev. Lett. **117**, 016602 (2016).

[17] H. Yuan, X. Zhou, Y. Cao, Q. Bian, Z. Zhang, H. Sun, S. Li, Z. Shao, J. Hu, Y. Zhu, Z. Mao, W. Ji, and M. Pan, Raman detection of hidden phonons assisted by atomic point defects in a two-dimensional semimetal, npj 2D Mater. Appl. **3**, 1 (2019).

[18] L. Muechler, A. Topp, R. Queiroz, M. Krivenkov, A. Varykhalov, J. Cano, C. R. Ast, and L. M. Schoop, Modular arithmetic with nodal lines: Drumhead surface states in ZrSiTe, Phys. Rev. X **10**, 011026 (2020).

[19] A. Topp, R. Queiroz, A. Grüneis, L. Müchler, A. W. Rost, A. Varykhalov, D. Marchenko, M. Krivenkov, F. Rodolakis, J. L. McChesney, B. V. Lotsch, L. M. Schoop, and C. R. Ast, Surface floating 2D bands in layered nonsymmorphic semimetals: ZrSiS and related compounds, Phys. Rev. X **7**, 041073 (2017).

[20] Y. Shao, A. Rudenko, J. Hu, Z. Sun, Y. Zhu, S. Moon, A. Millis, S. Yuan, A. Lichtenstein, D. Smirnov, Z. Mao, M. Katnelson, and D. Basov, Electronic correlations in nodal-line semimetals, Nat. Phys. **16**, 1 (2020).

[21] F. C. Chen, Y. Fei, S. J. Li, Q. Wang, X. Luo, J. Yan, W. J. Lu, P. Tong, W. H. Song, X. B. Zhu, L. Zhang, H. B. Zhou, F. W. Zheng, P. Zhang, A. L. Lichtenstein, M. I. Katnelson, Y. Yin, N. Hao, and Y. P. Sun, Temperature-Induced Lifshitz Transition and Possible Excitonic Instability in ZrSiSe, Phys. Rev. Lett. **124**, 236601 (2020).

[22] Y. Zhang, C. Wang, L. Yu, G. Liu, A. Liang, J. Huang, S. Nie, X. Sun, Y. Zhang, B. Shen, J. Liu, H. Weng, L. Zhao, G. Chen, X. Jia, C. Hu, Y. Ding, W. Zhao, Q. Gao, C. Li *et al.*, Electronic evidence of temperature-induced Lifshitz transition and topological nature in $ZrTe_5$, Nat. Commun. **8**, 1 (2017).

[23] Y. Liu, Y.-F. Liu, X. Gui, C. Xiang, H.-B. Zhou, C.-H. Hsu, H. Lin, T.-R. Chang, W. Xie, and S. Jia, Bond-breaking induced Lifshitz transition in robust Dirac semimetal VAI_3, Proc. Natl Acad. Sci. (USA) **117**, 15517 (2020).

[24] H. Yang, L. Yang, Z. Liu, Y. Sun, C. Chen, H. Peng, M. Schmidt, D. Prabhakaran, B. A. Bernevig, C. Felser, B. H. Yan, and Y. L. Chen, Topological Lifshitz transitions and Fermi arc manipulation in Weyl semimetal NbAs, Nat. Commun. **10**, 3478 (2019).

[25] F. Caglieris, C. Wuttke, S. Sykora, V. Süss, C. Shekhar, C. Felser, B. Büchner, and C. Hess, Anomalous Nernst effect and field-induced Lifshitz transition in the Weyl semimetals TaP and TaAs, Phys. Rev. B **98**, 201107(R) (2018).

[26] Y. Wu, N. H. Jo, M. Ochi, L. Huang, D. Mou, S. L. Bud'ko, P. C. Canfield, N. Trivedi, R. Arita, and A. Kaminski, Temperature-Induced Lifshitz Transition in WTe_2, Phys. Rev. Lett. **115**, 166602 (2015).

[27] M. Qi, C. An, Y. Zhou, H. Wu, B. Zhang, C. Chen, Y. Yuan, S. Wang, Y. Zhou, X. Chen, R. Zhang, and Z. Yang, Pressure-driven Lifshitz transition in type-II Dirac semimetal $NiTe_2$, Phys. Rev. B **101**, 115124 (2020).

[28] F. Liu, J. Li, K. Zhang, S. Peng, H. Huang, M. Yan, N. Li, Q. Zhang, S. Guo, X. Lü, P. Cai, L. Yin, S. Zhou, W. Duan, J. Shen, and W. Yang, Pressure-induced Lifshitz transition in the type II Dirac semimetal $PtTe_2$, Sci. China-Phys. Mech. Astron. **62**, 48211 (2019).

[29] N. Xu, Z. W. Wang, A. Magrez, P. Bugnon, H. Berger, C. E. Matt, V. N. Strocov, N. C. Plumb, M. Radovic, E. Pomjakushina, K. Conder, J. H. Dil, J. Mesot, R. Yu, H. Ding, and M. Shi, Evidence of a Coulomb-Interaction-Induced Lifshitz Transition and Robust Hybrid Weyl Semimetal in T_d-$MoTe_2$, Phys. Rev. Lett. **121**, 136401 (2018).

[30] S. Beaulieu, S. Dong, N. Tancogne-Dejean, M. Dendzik, T. Pincelli, J. Maklar, R. P. Xian, M. A. Sentef, M. Wolf, A. Rubio, L. Rettig, and R. Ernstorfer, Ultrafast dynamical Lifshitz transition, Sci. Adv. **7**, eabd9275 (2021).

[31] L. M. Schoop, M. N. Ali, C. Straßer, A. Topp, A. Varykhalov, D. Marchenko, V. Duppel, S. S. Parkin, B. V. Lotsch, and C. R. Ast, Dirac cone protected by non-symmorphic symmetry and three-dimensional Dirac line node in ZrSiS, Nat. Commun. **7**, 1 (2016).

[32] See Supplemental Material at http://link.aps.org/supplemental/10.1103/PhysRevB.103.205138 for a representative EDX spectrum, additional FFT spectra, and data from the 0.95 eV pump experiments.

[33] G. Kresse and J. Furthmüller, Efficiency of ab-initio total energy calculations for metals and semiconductors using a plane-wave basis set, Comput. Mater. Sci. **6**, 15 (1996).

[34] A. Togo and I. Tanaka, First principles phonon calculations in materials science, Scr. Mater. **108**, 1 (2015).

[35] W. Bensch and P. Dürichen, Structure of the layer compound ZrSiTe, Acta Cryst. C **50**, 346 (1994).

[36] S. Klemenz, A. K. Hay, S. M. Teicher, A. Topp, J. Cano, and L. M. Schoop, The role of delocalized chemical bonding in square-net-based topological semimetals, J. Am. Chem. Soc. **142**, 6350 (2020).